Int. J. Heat Mass Transfer. Vol. 22, pp. 1631–1643
© Pergamon Press Ltd. 1979. Printed in Great Britain

0017-9310/79/1201-1631 $02.00/0

APPLICATION OF A SECOND-MOMENT TURBULENCE CLOSURE TO HEAT AND MASS TRANSPORT IN THIN SHEAR FLOWS—I. TWO-DIMENSIONAL TRANSPORT

B. E. LAUNDER and D. S. A. SAMARAWEERA
University of California, Davis, CA 95616, U.S.A.

(*Received* 11 *December* 1978 *and in revised form* 8 *May* 1979)

Abstract—The paper presents developments of a second-moment approximation to turbulent convection in which the turbulent heat fluxes themselves form the subject of a set of transport equations. Closure at this level avoids the need to prescribe the turbulent Prandtl number which is the principal empirical uncertainty in simpler treatments. Applications are reported of heat transfer in a variety of free shear flows and boundary layers. While fairly successful overall agreement is achieved, the model does not fully account for the observed variations of turbulent Prandtl number from one free shear flow to another and equally gives rather inaccurate predictions downstream of a short heated patch in a wall.

NOMENCLATURE

C, mean temperature (or mass fraction of some passive contaminant);
C_o, maximum variation of C across shear flow;
C_w, wall value of C;
C_τ, 'friction' temperature, $q''_w/\rho U_\tau c_p$;
c, fluctuations in temperature about mean value;
$\bar{c}$, bulk average value mass fraction;
c_p, specific heat at constant pressure;
c_v, specific heat at constant volume;
D, diameter of pipe;
E, E_c, additive constants in sublayer wall laws [equations (14) and (15)];
k, turbulence kinetic energy;
P, mean static pressure;
p, fluctuation of static pressure about mean value;
R, ratio of velocities of slow-velocity:high-velocity streams in mixing layer;
r, pipe radius;
Re, Reynolds number based on pipe diameter and bulk mean velocity;
T, turbulent interaction timescale;
U_i, mean component of velocity in direction x;
U_o, maximum change in velocity across shear flow;
U_τ, friction velocity, $\sqrt{\tau_w/\rho}$;
u, fluctuation of x component of velocity about mean value;
u_i, fluctuation of x_i velocity component about mean value;
v, fluctuating component of velocity in y direction;
x, streamwise coordinate;
x_i, Cartesian coordinates;
y, coordinate normal to x in direction of principal gradients;
$y_{\frac{1}{2}}$, distance from symmetry plane at which velocity above or below external stream velocity is half of that on symmetry plane;
$y_{c\frac{1}{2}}$, distance from symmetry plane at which temperature above (or below) external temperature is half of that on symmetry plane.

Greek symbols

δ, boundary layer thickness;
ε, kinematic dissipation rate of kinetic energy;
ε_c, dissipation rate of $\overline{c^2}$;
η, similarity coordinate for mixing layer. Cross stream coordinate normalized by distance between points where velocity differs from the adjacent edge value by 10% of velocity change across layer;
η_c, similarity variable for scalar field corresponding to η for velocity field;
κ, Von Karman constant (0.42);
λ, thermal diffusivity;
ν, kinematic viscosity;
ρ, density;
σ_t, turbulent Prandtl number;
τ_w, wall shear stress.

1. INTRODUCTION

SECOND-ORDER or second-moment turbulence closures which originated with the work of Rotta [1] have been extensively used over the past decade for the numerical simulation of turbulent shear flows [2–4]. With turbulence models of this type, the second-moment correlations representing the turbulent transport of momentum, heat or any other scalar are found directly from their own (necessarily approximate) transport equations. The approach may be contrasted with the usual phenomenological treatment in which, by analogy with molecular transport, models are devised for

the effective turbulent viscosity and effective turbulent Prandtl or Schmidt number. The reason for preferring a second-moment model is that the turbulent interactions which generate the turbulent stresses and heat fluxes can be treated *exactly*: moreover, for those processes which cannot be so handled, a more rational and systematic set of approximations can be devised than for schemes founded on the notion of effective turbulent transport coefficients.

Applications of models of this type to shear flows of engineering interest have been largely limited to momentum transport processes. Hitherto, the only extensive studies of heat transport phenomena with second-moment models have been in relation to buoyancy dominated transport processes in the Earth's boundary layer, e.g. references [5–8]. These closures are especially appropriate to such flows for, as implied above, the direct effects of buoyancy on the second-moment correlations of interest enter explicitly in the system of turbulent transport equations. The outcome of such studies has, on the whole, been rather encouraging. In several cases experimentally observed phenomena, which would be simply impossible if turbulence were purely a gradient-driven process, have been at least qualitatively predicted.

It must be said, however, that experimental documentation of buoyancy dominated turbulence is at present neither particularly precise nor plentiful. The question therefore arises as to how well a second-moment model would fare in resolving some of the paradoxes observed in *well*-documented shear flows without buoyant contamination. It is this question that the present contribution addresses. The only earlier study to have considered the same question appears to be the Ph.D. thesis of Owen [9]. Owen confined attention to flows bounded by walls however, and in a number of respects made approximations which would fail badly in free shear flows. The present study examines several free shear flows as well as cases of pipe and channel flow and the developing thermal boundary layer. Attention is limited to two-dimensional or axisymmetric flows, however. A companion paper [10] reports an extension of the scheme to two problems of three-dimensional convection. The closure proposals adopted in this study have in most respects appeared elsewhere in the literature. Except for the points of novelty therefore, Section 2 provides only a brief presentation of the mathematical model and the method of numerical solution. Comparison between model simulation and experiments is provided in Section 3, while an overall assessment is attempted in Section 4.

2. THE PHYSICAL AND MATHEMATICAL MODEL

a. *The turbulence model*

The instantaneous Navier–Stokes and energy equations for a low-speed flow of fluid with uniform density and transport properties may be written

$$\frac{\partial(U_i+u_i)}{\partial t}+\frac{\partial}{\partial x_j}(U_i+u_i)(U_j+u_j) = -\frac{1}{\rho}\frac{\partial}{\partial x_i}(P+p)+\nu\frac{\partial^2(U_i+u_i)}{\partial x_j^2} \quad (1)$$

$$\frac{c_v}{c_p}\frac{\partial(C+c)}{\partial t}+\frac{\partial}{\partial x_j}(C+c)(U_j+u_j) = \lambda\frac{\partial^2(C+c)}{\partial x_j} \quad (2)$$

wherein upper-case letters distinguish mean components of velocity, pressure, and temperature (U, P, and C) from the corresponding turbulent fluctuations about the mean, denoted by lower-case letters. Other symbols appearing in equation (1) and (2) take their conventional meanings: definitions are provided under the Section headed Nomenclature.

Conventional time averaging of equation (1) and (2) over a period that is long compared with that of a typical large scale turbulent fluctuation produces for a statistically stationary flow

$$\frac{\partial U_iU_j}{\partial x_j}=\frac{1}{\rho}\frac{\partial P}{\partial x_j}+\frac{\partial}{\partial x_j}\left(\nu\frac{\partial U_i}{\partial x_j}-\overline{u_iu_j}\right) \quad (3)$$

$$\frac{\partial CU_j}{\partial x_j}=\frac{\partial}{\partial x_j}\left(\lambda\frac{\partial C}{\partial x_j}-\overline{cu_j}\right). \quad (4)$$

Exact transport equations for the as-yet unknown second-moment correlations in equations (3) and (4) are obtained as follows: Equation (1) is multiplied by u_k and to this is added the same equation but with subscripts i and k interchanged. Upon averaging, the following transport equation for $\overline{u_iu_k}$ is produced:

$$\begin{aligned}\frac{\partial}{\partial x_j}U_j\overline{u_iu_k} = &-\left\{\overline{u_iu_j}\frac{\partial U_k}{\partial x_j}+\overline{u_ku_j}\frac{\partial U_i}{\partial x_j}\right\}\\ &+\overline{\frac{p}{\rho}\left(\frac{\partial u_i}{\partial x_k}+\frac{\partial u_k}{\partial x_i}\right)}-2\nu\overline{\frac{\partial u_i}{\partial x_j}\frac{\partial u_k}{\partial x_j}}\\ &-\frac{\partial}{\partial x_j}\left(\overline{u_iu_ju_k}+\overline{\frac{pu_i}{\rho}}\delta_{jk}\right.\\ &\left.+\overline{\frac{pu_k}{\rho}}\delta_{ik}-\nu\frac{\overline{\partial u_iu_k}}{\partial x_j}\right).\end{aligned} \quad (5)$$

The corresponding equation for $\overline{cu_i}$ is obtained by adding equation (1) multiplied by c to equation (2) multiplied by u_i. The resultant equation may be rearranged as

$$\begin{aligned}\frac{\partial}{\partial x_j}(U_j\overline{u_ic}) = &-\left\{\overline{u_iu_j}\frac{\partial C}{\partial x_j}+\overline{cu_j}\frac{\partial U_i}{\partial x_j}\right\}\\ &+\overline{\frac{p}{\rho}\frac{\partial c}{\partial x_i}}-(\lambda+\nu)\overline{\frac{\partial u_i}{\partial x_j}\frac{\partial c}{\partial x_j}}\\ &-\frac{\partial}{\partial x_j}\left(\overline{u_iu_jc}+\overline{\frac{pc}{\rho}}\delta_{ij}\right.\\ &\left.-\lambda u_i\overline{\frac{\partial c}{\partial x_j}}-\nu c\overline{\frac{\partial u_i}{\partial x_j}}\right).\end{aligned} \quad (6)$$

Equations (5) and (6) are not immediately employable to find $\overline{u_i u_k}$ and $\overline{u_i c}$ since their right hand sides contain still further unknowns. In a second-moment closure these unknown correlations must be approximated in terms of the mean field distributions of velocity and temperature, the turbulent stress and heat fluxes, and a number of characteristic time scales (usually one) to characterize the rate at which the various turbulence interactions proceed.

In the present study the Reynolds stress field has been obtained using strictly the closure presented in [4]. Here therefore, the set of algebraic relations is simply presented in Table 1 without further comment. The question of closing the corresponding heat flux equation [equation (6)] has been examined in detail in [11]. The specific approximations and the underlying ideas are considered briefly below.

At high turbulent Peclet numbers the terms in equation (5) containing the molecular transport coefficients are negligible. For fluids with Prandtl numbers of order unity or greater their omission is entirely admissible except in the immediate vicinity of wall (say, for $y^+ < 30$). In analyzing wall flows in the present work we use a correlation of experimental data to span this near-wall sublayer. The first pair of terms on the RHS of equation (6), representing the generative action of mean temperature and velocity gradients, requires no approximation since it contains only the second moments of interest and the mean field variables. For these shear flows the next term, the pressure–temperature gradient correlation, is far and away the most crucial term to approximate. There are basically two different types of processes to be represented, one arising from purely turbulence interactions and a second due to the presence of mean strain [11]: these interactions are denoted by $\phi_{ic,1}$ and $\phi_{ic,2}$ respectively. There is a further influence for flows along a rigid boundary associated with pressure reflections from the wall, $\phi_{ic,w}$. Thus symbolically:

$$\overline{\frac{p}{\rho}\frac{\partial c}{\partial x_i}} = \phi_{ic,1} + \phi_{ic,2} + \phi_{ic,w}. \tag{7}$$

Following Monin [12] and nearly all subsequent workers we take

$$\phi_{ic,1} = -c_{1c}\frac{\overline{u_i c}}{T} \tag{8}$$

where T is a time scale and c_{1c} is assumed to be a constant. In reference [11] it was suggested that the most appropriate time scale with which to characterize this process would be $(k\overline{c^2}/\varepsilon\varepsilon_c)^{1/2}$ where ε_c is the dissipation rate of $\overline{c^2}$. At present, however, there appears to be no well-tested scheme for obtaining ε_c: in the present work therefore the time scale in equation (8) is taken as k/ε, i.e. the scalar time scale of the

Table 1. Model of ref. [4] for calculating the Reynolds stress field

$$\overline{\frac{p}{\rho}\left(\frac{\partial u_i}{\partial x_j}+\frac{\partial u_j}{\partial x_i}\right)} = \phi_{ij,1} + \phi_{ij,2} + \phi_{ij,w}$$

where

$$\phi_{ij,1} = -c_1\frac{\varepsilon}{k}\left(u_i u_j - \frac{2}{3}\delta_{ij}k\right)$$

$$\phi_{ij,2} = -\frac{(c_2+8)}{11}\left(P_{ij}-\frac{\delta_{ij}}{3}P_{kk}\right) - \frac{(30c_2-2)}{55}k\left(\frac{\partial U_i}{\partial x_j}+\frac{\partial U_j}{\partial x_i}\right) - \frac{(8c_2-2)}{11}\left(D_{ij}-\frac{1}{3}\delta_{ij}D_{kk}\right)$$

and

$$P_{ij} \equiv -\left\{\overline{u_i u_k}\frac{\partial U_j}{\partial x_k} + \overline{u_j u_k}\frac{\partial U_i}{\partial x_k}\right\}; \qquad D_{ij} \equiv -\left\{\overline{u_i u_k}\frac{\partial U_k}{\partial x_j} + \overline{u_j u_k}\frac{\partial U_k}{\partial x_i}\right\}$$

$$\phi_{ij,w} = \left[c_1'\frac{\varepsilon}{k}\left(\overline{u_i u_j} - \frac{2}{3}\delta_{ij}k\right) + c_2'(P_{ij}-D_{ij})\right]\frac{k^{3/2}}{\varepsilon x_n}$$

$c_1 = 1.5$; $c_2 = 0.4$; $c_1' = 0.125$; $c_2' = 0.015$

$$\nu\overline{\frac{\partial u_i}{\partial x_k}\frac{\partial u_j}{\partial x_k}} = \frac{2}{3}\delta_{ij}\varepsilon \qquad \overline{\frac{pu_j}{\rho}} = 0$$

$$-\overline{u_i u_j u_k} = c_s\frac{k}{\varepsilon}\left(\overline{u_i u_l}\frac{\partial \overline{u_j u_k}}{\partial x_l} + \overline{u_j u_l}\frac{\partial \overline{u_k u_i}}{\partial x_l} + \overline{u_k u_l}\frac{\partial \overline{u_i u_j}}{\partial x_l}\right)$$

$c_s = 0.11$

turbulent *velocity* field. Implications and limitations of this assumption are discussed in the following section.*

The mean strain contribution, $\phi_{ic,2}$, has been neglected in many closure schemes, e.g. [2, 3, 7]. Two other models have been in common use, the *quasi-isotropic* model [13]

$$\phi_{ic,2} = +0.8\overline{u_k c}\frac{\partial U_i}{\partial x_k} - 0.2\overline{u_k c}\frac{\partial U_k}{\partial x_i} \quad (9)$$

and the *destruction of production* hypothesis

$$\phi_{ic,2} = c_{2c}\overline{u_k c}\frac{\partial U_i}{\partial x_k}. \quad (10)$$

In the limit of vanishingly small anisotropy, equation (9) may be shown to be exactly correct. For the highly sheared flows considered in this work, however, it provides a less satisfactory approximation than equation (10). Here therefore, calculations are presented only for the latter form with the empirical coefficient c_{2c} taking the optimized value 0.4, i.e. 40% of the heat flux production due to mean strain is assumed obliterated by pressure interactions. Equation (10) has previously been used in [9] and [11] with c_{2c} taking the value 0.5: the present somewhat lower value gives minor improvements in the calculated levels of streamwise turbulent heat flux. Although this flux is not important in the thin shear flows considered here (being swamped by streamwise *convection*) its effects may be significant in recirculating flows.

Although the wall-reflection effect on the heat fluxes does not seem as pronounced as on the Reynolds normal stresses, contrary to what had been tentatively suggested in [11], it is not entirely negligible. Two schemes for approximation have been tried, one of which is the recent proposal of Gibson and Launder [8] for analysing turbulence in the Earth's boundary layer. For thin shear flows near a single plane wall unaffected by buoyancy their scheme reduces to the form

$$\phi_{ic,w} = c'_{c1,w}\overline{u_k c}n_k n_i \frac{k^{3/2}}{\varepsilon x_n} \quad (11)$$

where n_k is the unit vector normal to the wall, x_n is the normal distance from the wall and the coefficient $c'_{c1,w}$ takes the value 0.25. The second formulation, evolved in the present work, was designed to parallel as closely as possible, the near-wall pressure-reflection model for the Reynolds stresses, $\phi_{ij,w}$, given in Table 1. The form adopted was

$$\phi_{ic,w} = \left\{ -c_{c1,w}\frac{\varepsilon}{k}\overline{u_i c} - \beta'\overline{u_i c}\left(4\frac{\partial U_i}{\partial x_{il}} - \frac{\partial U_l}{\partial x_i}\right)\right\}\frac{k^{3/2}}{\varepsilon x_n}. \quad (12)$$

The coefficients $c_{c1,w}$ and β'_c have been given the values 0.1 and 0.02 to bring accord with the levels of heat fluxes normal to the wall and in the streamwise direction in an equilibrium flow near a wall.

For the case of flow in straight ducts, pipes or subchannels where surfaces may be non-planar the effective distance from the wall must usually be found by integration. From several possible forms the following has been chosen as the most plausible simple expression:

$$\frac{1}{x_n} = \frac{1}{2}\int_0^{2\pi}\frac{\mathrm{d}\theta}{l}$$

where l is the length of the line joining the point in question to a point on the surface, and θ is the angle subtended between this line and some reference line. With this form, for the case of an infinite plane wall the original expression is recovered. In the case of a circular sectioned pipe of radius R, the following expression is obtained:

$$\frac{1}{x_n} = \frac{1}{2R}\int_0^{\pi}\frac{(1 - b\cos\theta)\mathrm{d}\theta}{(1 + b^2 - 2b\cos\theta)^{3/2}}$$

where $b = (R - y)/R$, y being the distance from the pipe wall. The diffusion terms in equation (6) are approximated as

$$-\left(\overline{u_i u_j c} + \frac{\overline{pc}}{\rho}\delta_{ij}\right) = c_c\frac{k}{\varepsilon}\left(\overline{u_k u_l}\frac{\partial\overline{u_i c}}{\partial x_l} + \overline{u_i u_l}\frac{\partial\overline{u_j c}}{\partial x_l}\right). \quad (13)$$

The above form appeared to give the best overall agreement among several versions considered, cf. [11]: the predictions, however, were only marginally different for the different flows examined here provided the single empirical coefficient was appropriately chosen. By analogy with the stress-diffusion model shown in Table 1 the c_c has been taken as 0.11. This may not represent the *best* value, though it is unlikely to differ by more than about 50% from the optimum.†

b. *Solution of equations*

Use of the model of turbulence described above for heat transport in two-dimensional or axisymmetric thin shear flows requires solution of transport equations for the Reynolds stresses $\overline{u_1^2}$, $\overline{u_2^2}$, $\overline{u_3^2}$, and $\overline{u_1 u_2}$ (x_1 denoting the streamwise direction and x_2 the direction of principal gradient of velocity and temperature), for the energy dissipation rate ε and for the turbulent heat flux $\overline{u_2 c}$, in addition to the dependent variables for the mean field. In addition, the streamwise heat flux $\overline{u_1 c}$ is calculated according to the model proposals since it is an easier quantity to measure than $\overline{u_2 c}$ and has

* Lumley [37] has recently constructed the framework of a far more comprehensive approximation of $\phi_{ic,1}$ than is attempted here.

† Again, more elaborate treatments of the transport terms are available in the literature [37]. Our view is that the particular set of flows examined here does not allow a decisive choice to be made among the different strategies owing to the uncertainties in modelling the other, more influential interactions.

frequently been reported in the literature. [Comparisons with this streamwise heat flux provides an important test of the process denoted by $\phi_{ic,2}$ since there is no contribution from equation (10) in the equation for u_2c.]*

In the diffusive terms on the right-hand sides of the transport equations for turbulence variables only the cross-stream component is of significance; a parabolic 'marching' solution may therefore be adopted. We have used the widely known finite-difference method of Patanakar and Spalding [15] as the basis for the numerical solution. The original scheme was formulated for use with an 'effective viscosity' scheme for modelling turbulent transport however, and thus a number of modifications to the basic structure had to be introduced in the present work. The most important of these was the decision to stagger the location of nodes for the turbulence variables relative to mean-field nodes. This staggering saved a modest amount of computer time (since fewer interpolations were involved) and, more importantly, rendered the system of equations highly stable.† Typically 22 nodes across the shear flow were used. At the initial station these were distributed so as just to cover the region of interest; as the calculation proceeded downstream the width of the grid adjusted so as to enclose all the flow domain with significant gradients in at least one of the dependent variables. Solution of these equations for a typical flow required about 6 s execution time on a CDC 7600. Thus, despite the relative complexity of the model, it is economically feasible to use the scheme for studying practically interesting engineering flows.

In most of the flows studied the calculated flow pattern achieved an asymptotic form that was independent of the initially prescribed distribution of dependent variables. In the two non-equilibrium flows where the initial, *non-equilibrium* region was the focus of study, the heat (or mass) transfer did not begin until well downstream of the hydrodynamic origin of the shear flow. Accordingly, none of the differences between experiment and calculation can be attributed to uncertainties in initial conditions.

The following practices were followed in applying boundary conditions: At a plane or axis of symmetry the values of $\overline{u_2c}$ and $\overline{u_1u_2}$ are set to zero while the normal gradient of all other dependent variables is made to vanish there. At a quiescent free-stream edge the temperature and velocity are set equal to their free-stream values, the heat fluxes are set to zero while very small positive levels of turbulence energy and energy dissipation rate are assigned, the distribution of energy among the components being isotropic.

As indicated in Section 2a, calculations of flow past walls did not enter the very thin sublayer adjacent to the wall where molecular transport is important. Instead the dependent variables were assumed to reach local-equilibrium values just outside the sublayer. Details for the Reynolds stresses and are given in [4]; for the thermal field

$$-\overline{u_2c} = \dot{q}''_w/\rho c_p - \lambda\frac{\partial C}{\partial x_2}$$

while for the streamwise flux

$$\overline{u_1c} = -\text{constant}\ x\overline{u_2c}$$

where the magnitude of the constant is chosen to be compatible with the particular near-wall correction used, i.e. equations (11) or (12). Finally a link between the wall temperature and heat flux is provided by the semi-logarithmic law

$$\frac{(C - C_w)}{C_\tau} = \frac{1}{\kappa'}\ln E_c x_2^+ \tag{14}$$

where κ' takes the value 0.465 and E_c is an empirical function of Prandtl number correlated (in somewhat different form) by Jayatilleke [17]. The present study has considered only air at low temperatures for which the recommended value of E_c is 4.75.

For the mean velocity field an entirely analogous relation is adopted

$$\frac{U_1}{U_\tau} = \frac{1}{\kappa}\ln Ex_2^+ \tag{15}$$

where κ and E take the (constant) values 0.42 and 11.0 respectively.

3. PRESENTATION AND DISCUSSION OF RESULTS

Comparisons are made first with three types of free shear flow and subsequently with flows near walls. To simplify presentation we now revert to the usual x, y, z notation for Cartesian coordinates with corresponding velocity fluctuations u, v and w. Throughout, x denotes the principal flow direction and y the direction of significant velocity and temperature gradients.

The first case is that of the plane jet in stagnant surroundings. The hydrodynamic properties of this flow have been compared (and shown to be in good agreement) with the present closure in [4]: attention is here limited to the thermal characteristics. The mean temperature field has been reported *inter alia* by Van der Hegge Zijnen [18] and Jenkins and Goldschmidt [19]. The calculated behaviour shown in Fig. 1 displays essentially complete agreement with the measured behaviour as does, likewise, the turbulent heat flux $\overline{vc}$. The turbulent Prandtl number shown in Fig. 2 displays a nearly uniform level of about 0.6 over the inner half of the profile, rising steadily over the outer half of the jet.

Comparisons with the plane wake are complicated by the fact that the level of shear stress shown in Fig. 3 is generally predicted too low, so the flow spreads too

* If equation (9) rather than (10) were used, solution of the equation for $\overline{u_1c}$ would be mandatory due to the resultant intercoupling of the heat fluxes.

† A number of workers had previously found that mean velocity profiles tended to develop a saw-tooth variation when the shear stress was evaluated at the same positions as the mean velocities (e.g. Launder and Morse [16]).

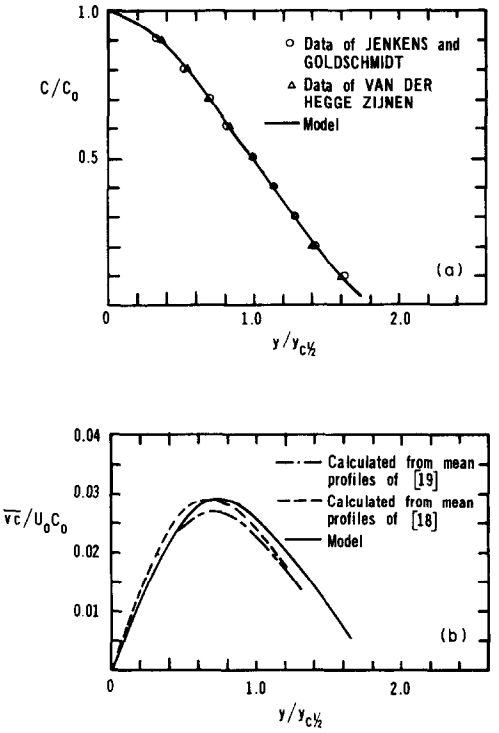

FIG. 1. Thermal development of turbulent plane jet in stagnant surroundings. (a) Mean temperature profiles, (b) Lateral heat flux profiles.

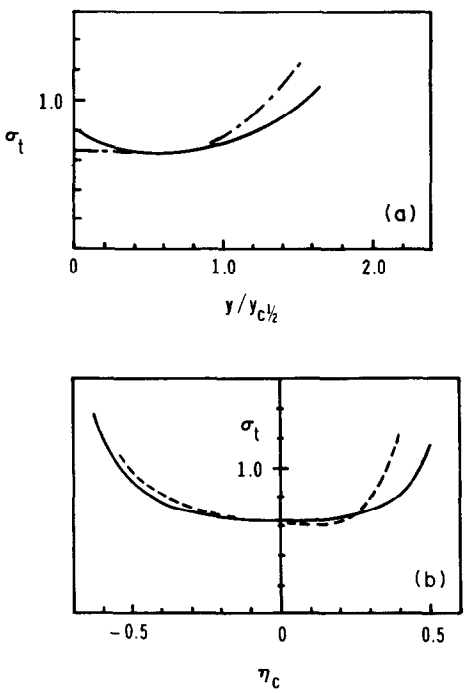

FIG. 2. Calculated distribution of turbulent Prandtl number in free shear flows. (a) Plane jet (——) and plane wake (– – –), (b) Plane mixing layers: $R = 0.5$ (——); $R = 0$. (– – –).

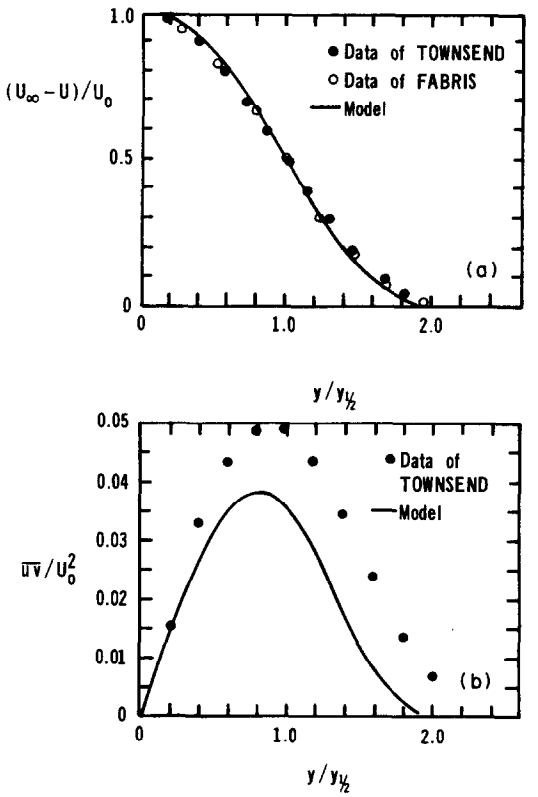

FIG. 3. Flow field characteristics of the plane turbulent wake. (a) Mean velocity, (b) Turbulent shear stress.

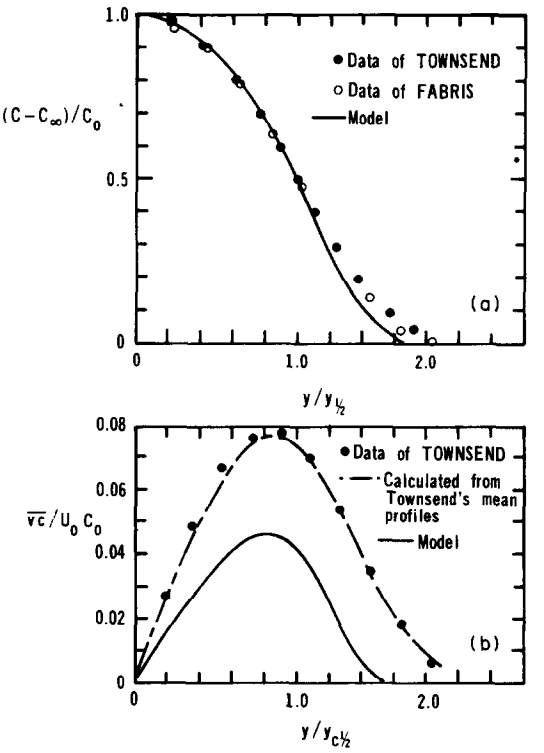

FIG. 4. Thermal characteristics of the plane turbulent wake. (a) Mean temperature profile, (b) Lateral heat flux profiles.

slowly: moreover, near the outer edge of the wake the shear and normal stresses fall to zero too quickly. These features naturally influence, in entirely foreseeable ways, the mean temperature and heat flux profiles which are compared with the measurements of Townsend [20] in Fig. 4. Fabris [21] has also made a detailed study of the thermal wake, though his data do not appear to have extended far enough downstream for self-preserving levels of heat fluxes to have been reached. It seems likely that the ratio of the heat fluxes are, however, insensitive to whether precisely self-preserving conditions have been reached; the present predictions of this ratio shown in Fig. 5 are in generally good agreement with the data. The calculated turbulent Prandtl number variation shown in Fig. 2 exhibits a distribution rather similar to that of the plane jet though attaining somewhat lower values near the plane of symmetry and somewhat higher levels in the outer region. Although no detailed profiles of turbulent Prandtl number across a wake appear to have been reported in the experimental literature the average level obtained in the present calculations is essentially correct since the ratio of the half widths of the scalar and velocity distributions, 1.16, is the same as measured by Fabris.

The scalar and velocity fields of a plane mixing layer with a velocity ratio of 0.5 have been extensively documented by Watt [22]. Computations of the velocity field (which so far as we know have not been reported) are shown in Figs. 6 and 7. Agreement of mean velocity and Reynolds stresses is generally close though we notice that the calculated turbulent normal stresses fall to zero more rapidly than the measurements towards the high velocity edge. As a consequence of this, the turbulent heat flux shown in Fig. 8 also falls abruptly to zero: despite this shortcoming, however, the mean temperature field shown in Fig. 9 is satisfactorily predicted. The measured ratio of the rates of spread of the thermal and velocity layers is 1.13, a figure that the present calculations match within 2%.

Agreement is less satisfactory for the mixing layer generated between a moving stream and a stationary fluid. There have been many flow-field studies of this configuration which served to emphasize how sensitive is the spreading rate to the details of the experimental

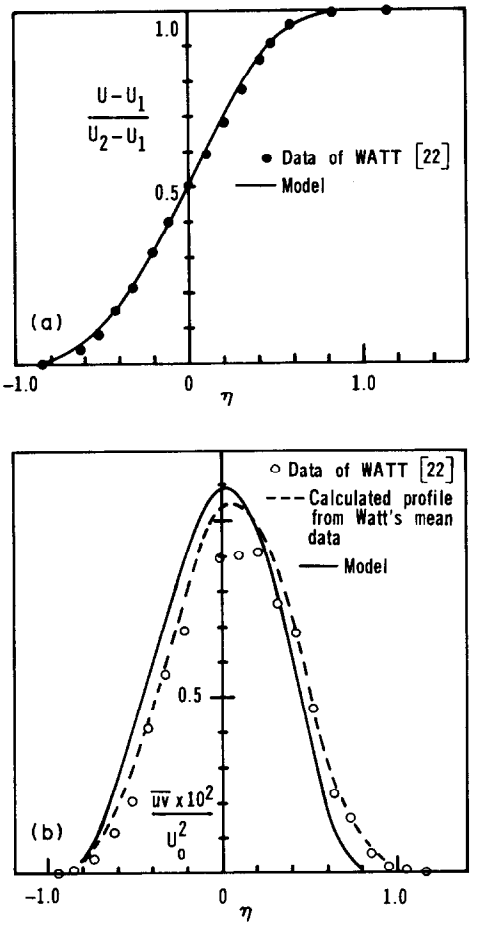

FIG. 6. Flow field characteristics of plane mixing layer with velocity ratio $R = 0.5$. (a) Mean velocity profile, (b) Shear stress profiles.

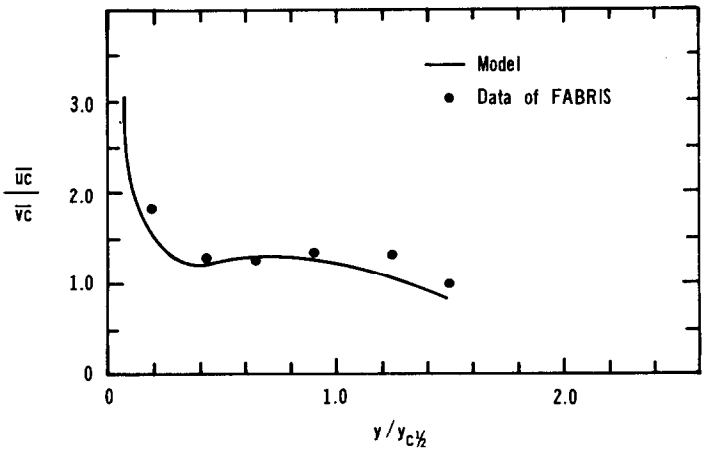

FIG. 5. Ratio of streamwise: lateral heat fluxes in plane wake.

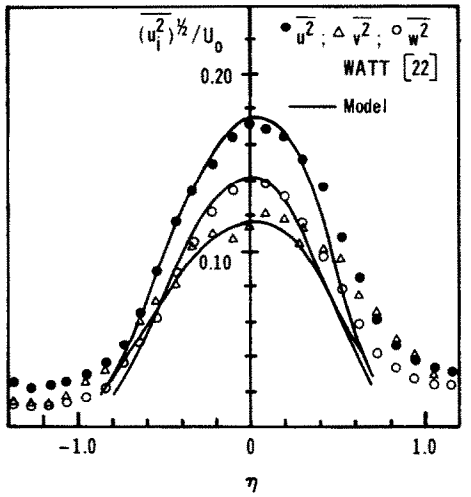

FIG. 7. Turbulence intensity profiles in plane mixing layer, $R = 0.5$.

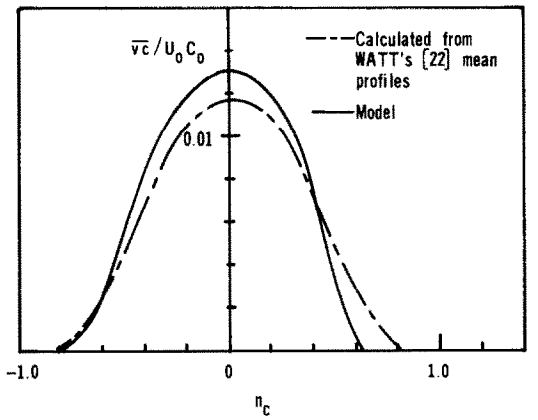

FIG. 8. Lateral turbulent heat flux in plane mixing layer, $R = 0.5$.

apparatus (cf. the review by Rodi [23]). The shear-layer spreading rate $d\delta_{0.9}/dx_1$ for the experiment by Sunyach and Mathieu [24] is 0.175 which is approx. 10% greater than predicted by the present model (and also about 10% greater than the mean spreading rate of the experiments reviewed in [23]). We might thus anticipate that the measured development of the temperature field (the moving stream being at a higher temperature than the surroundings) would likewise show a rate of growth some 10% too large. However, the measured thermal spreading rate $d\Delta_{2c}/dx$ of 0.249 is fully 25% larger than the calculations, while from Fig. 10 we see that the mean temperature shows a much too abrupt change of slope near the high-temperature (moving) edge. A similar though less pronounced defect is present in the mean velocity field (cf. the mixing layer predictions in [4]). Evidently, the sharp peaking of the turbulent Prandtl number shown in Fig. 2b (implying a decrease in effective thermal conductivity near the edges relative to the effective viscosity), while bringing accord with observed temperatures near the stationary edge, has exacerbated the problem near the high-temperature boundary.

We now consider three cases of flow near a wall, the first being that of fully developed flow in a circular-sectioned pipe. The calculated profiles of mean velocity and Reynolds stresses are shown by Samaraweera [25] to be in generally satisfactory agreement with the two principal experimental studies, those of Laufer [26] and Lawn [27]. The calculations involving a non-isothermal flow have attempted to simulate the experiments of Bremhorst and Bullock [28, 29] at a Reynolds number of 34 200 in which a uniform heat flux was prescribed at the wall. The distributions of mean temperature shown in Fig. 11 display close agreement with measurement, the profiles for the two different wall-effect functions bracketing the experimental data. The axial component of heat flux $\overline{uc}$ which appears in Fig. 12 is in highly satisfactory accord with the measurements: the two different wall-effect functions [equations (11) and (12)] give slightly different near-wall distributions, though for this particular case it is difficult to distinguish which version is the better.

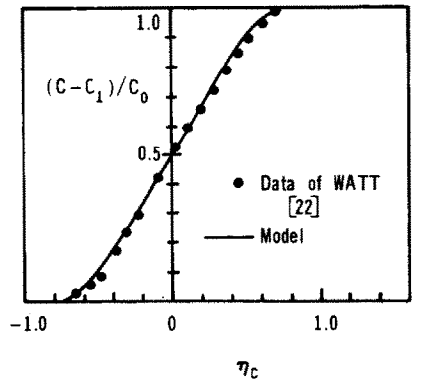

FIG. 9. Mean temperature distribution in plane mixing layer, $R = 0.5$.

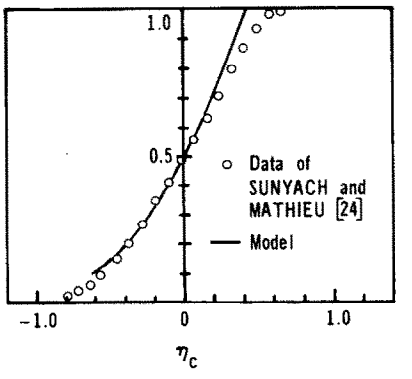

FIG. 10. Mean temperature profile in plane mixing layer in stagnant surroundings, $R = 0.0$.

The calculated distribution of turbulent Prandtl number shown in Fig. 13 displays a nearly uniform level of about 0.9 near the pipe wall falling to a value just over 0.6 at the axis. This is a similar distribution to that recommended for calculating heat transport in boundary layers; Rotta [30], for example, proposes $Pr_t = 0.9 - 0.5(y/\delta)$, δ being the boundary layer thickness.

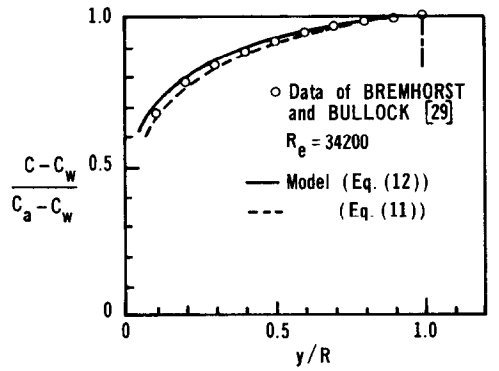

FIG. 11. Mean temperature profile in fully developed pipe flow.

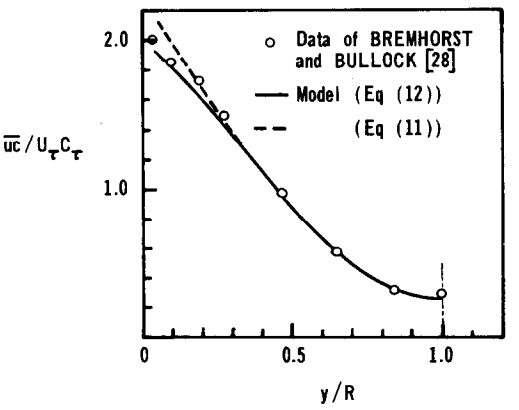

FIG. 12. Streamwise heat fluxes in fully developed pipe flow.

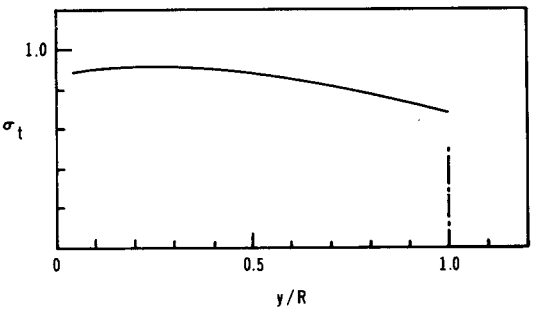

FIG. 13. Calculated profile of turbulent Prandtl number in fully developed pipe flow.

Figures 14 and 15 also relate to fully developed hydrodynamic flow in a pipe but now with the very different scalar boundary conditions studied by Quarmby and Anand [31]. A short porous ring, nominally 1.5 diameters in length, was inserted in the pipe and through this a foreign gas was injected at sufficiently low flow rates for the velocity field to be negligibly affected. Measured concentration profiles were obtained at the downstream end of the injection region ($x/D = 1.49$) and at four other stations as indicated in Fig. 14. The computations of this flow began *upstream* of the injection patch and exhibit excellent agreement at the first station. Thereafter, however, the calculated level of concentration at the wall falls more rapidly than do the measurements due to a more rapid radial dispersal of the tracer gas. Evidently, the predicted turbulent thermal conductivity is too high (by about 15%) or, equivalently, the turbulent Schmidt number is too low. The development of the latter parameter is shown in Fig. 15. As the foreign gas disperses towards the pipe axis the calculated turbulent Schmidt number falls to around 0.8 near the wall and to levels below unity wherever there are significant concentration gradients. Quarmby and Anand [31] in fact achieved closer agreement between their computations and measured behavior than that obtained in the present study by choosing a Schmidt number equal to unity throughout. The main

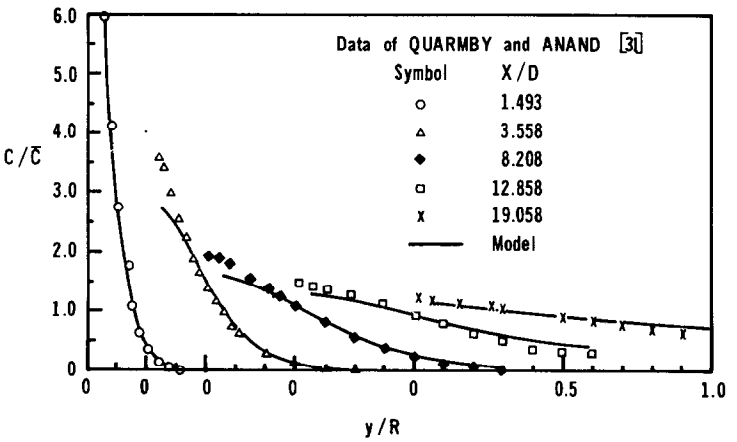

FIG. 14. Development of concentration profiles downstream of a short region of mass transfer through the pipe wall.

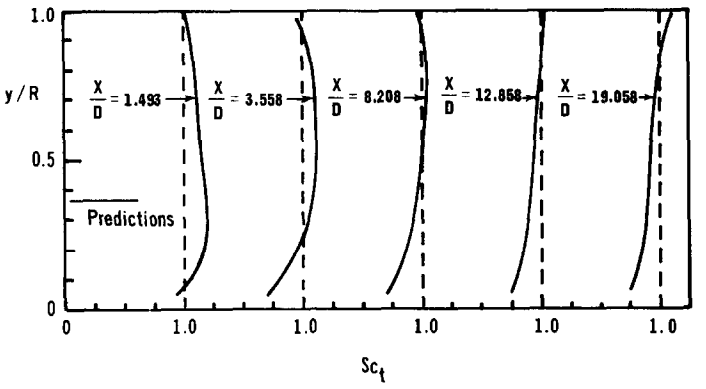

FIG. 15. Development of profiles of turbulent Schmidt number downstream of short region of mass transfer at pipe wall.

cause for the relatively poor agreement obtained with the present closure appears to be the choice of the turbulence energy turnover time (k/ε) as the characteristic time scale in the heat flux equation: the topic is discussed further in Section 4.

The final flow considered is that of a thermal boundary layer growing on a flat plate where an initial portion of the plate is unheated. Far enough from the start of heating the thermal layer will grow to the same thickness as the velocity shear layer; distributions of turbulent Prandtl number and other thermal characteristics will then become rather similar to the case of fully developed pipe flow. The present interest, however, is with the initial region immediately after the step in heat flux, where the thermal layer is thin, and for which Antonia, Danh and Prabhu [32] have recently reported extensive turbulence data. The distributions of heat fluxes $\overline{vc}$ and $\overline{uc}$ across the thermal boundary layer presented in Fig. 16 exhibit generally satisfactory agreement. The streamwise heat flux pro-

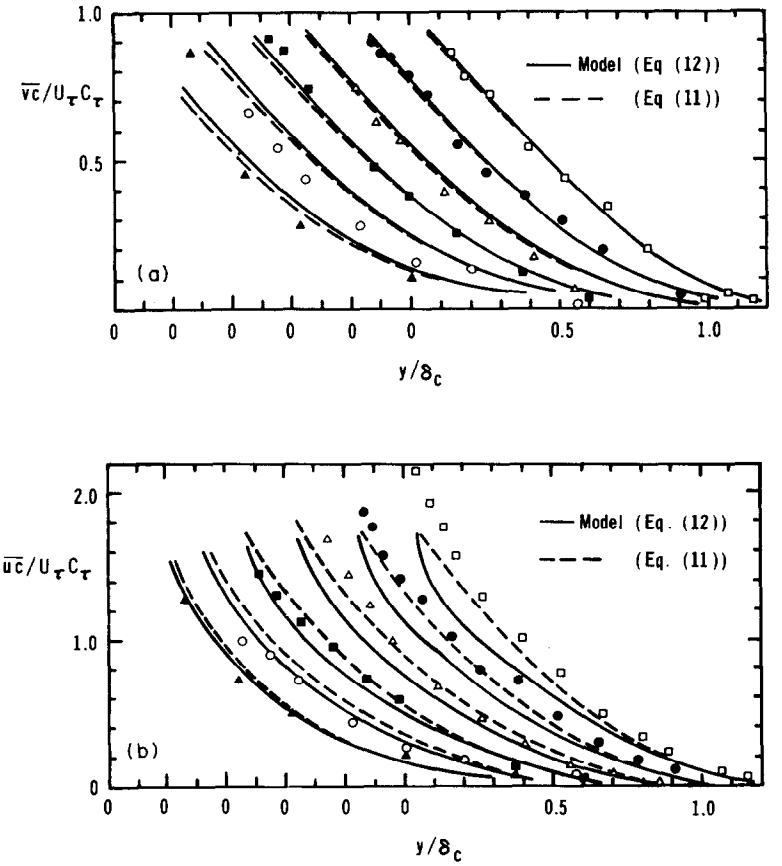

FIG. 16. Turbulent heat fluxes in turbulent boundary layer with step in wall heat flux (for key to symbols see Fig. 17). (a) Lateral heat fluxes, (b) Streamwise heat fluxes.

files suggest that equation (11) provides a somewhat more satisfactory near-wall correction than equation (12) while, for the flux normal to the wall, the two schemes produce essentially the same profiles. There is less satisfactory accord with the mean temperature profiles shown in Fig. 17. There are really two types of near-wall discrepancy. The first is that the coefficient E_c which appears in the near-wall boundary-condition for the temperature [equation (14)] is not constant when the thermal boundary layer is very thin. This feature does not seem to have been reported before (Antonia *et al.* [32] did not present their results in this form) though one may remark that the direction of the variation seems to accord with an effect on the *velocity* profiles found in low-Reynolds-number pipe flow [33] and in boundary layers formed between converging plane walls [34]. In these cases it is found that when there is a significant decrease in total shear stress across the viscosity-dependent region (greater than about 5%) there is a substantial increase in the constant E in equation (15). In the present case there is a decrease in heat flux across this sublayer and we likewise observe an increase in E_c. We do not at this stage attempt to prove that the former causes the latter though the fact that the experimental near-wall temperatures gradually approach the predicted line with passage downstream is at least consistent with this idea (i.e. the thermal layer thickness δ_c increases with x and thus gradients of heat flux normal to the plate become less steep). This defect in predicting the temperature profile arises in the boundary condition and it is thus not one that can properly be levelled at the present model which is concerned only with the high Reynolds number region.

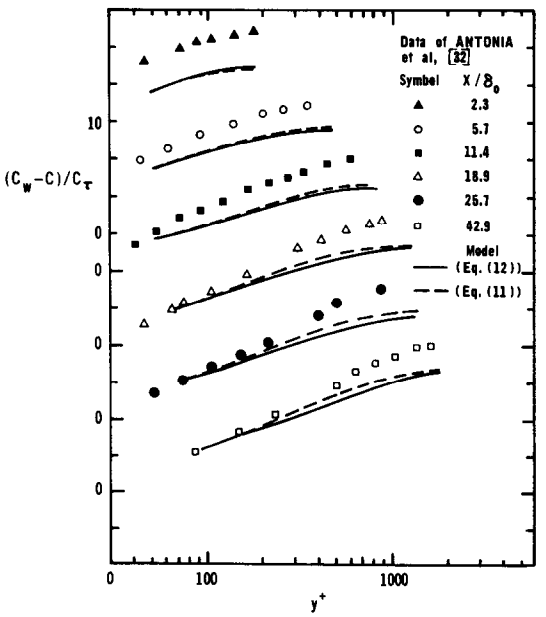

FIG. 17. Mean temperature profiles in flat plate boundary layer with step in wall heat flux.

Another difference that becomes particularly evident at the later stations is that the slope of the measured temperature profile is markedly greater than the calculated one. This suggests that the predicted thermal diffusivity is too high or, equivalently, the turbulent Prandtl number too low. Figure 18 confirms that the predicted level of σ_t at the final station is indeed lower than the measured levels by 15–60%. Included on this figure, however, are experimental data from the earlier studies of Fulachier [35] and Blom [36] of nominally the same flow* and these measurements are in much closer agreement with the present calculation. While it does not seem possible to isolate the origin of this difference between the experiments of [31] and the other cited cases it may be relevant that levels of turbulent shear stress and heat flux measured by Antonia *et al.* [31] are too low by some 25 and 20% respectively to support the experimentally observed growth of the boundary layer. The suggestion seems to be that the flow is converging (possibly due to the formation of boundary layers on the side wall of the wind tunnel) though it is not obvious why this should lead to abnormally high levels of turbulent Prandtl number. Ultimately, further experiments may be needed to resolve the paradox.

4. CONCLUDING REMARKS

The previous section has considered the prediction of heat or scalar transport in a variety of two dimensional shear flows. Generally, the second-moment turbulence closure used for the calculations has achieved an encouraging level of agreement. Nevertheless, detailed differences have emerged in the course of comparing calculation with experiment; it is appropriate therefore to close by noting directions in which the current model may be improved.

The most serious conceptual weakness is the ab-

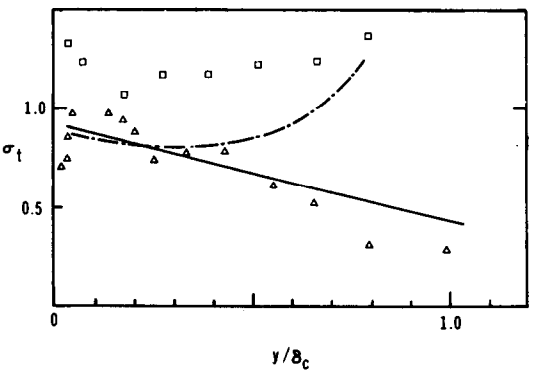

FIG. 18. Turbulent Prandtl number distribution in flat plate boundary layer. □ Data of Antonia *et al.* [32] at $x/\delta_0 = 42.9$, △ data of Blom [36], (· – · –) data of Fulachier [35], (——) present predictions.

* Fulachier studied the development downstream of a step in wall *temperature*. In turbulent flow however we may expect this to produce negligibly different profiles than arise for a step in heat flux.

sence of a timescale that is properly characteristic of the fluctuating scalar field like $\overline{c^2}/\varepsilon_c$. In the case of diffusion from a ring source examined in Fig. 14, the production rate of $\overline{c^2}$ falls dramatically downstream of the source because mean scalar gradients near the wall are then small (cf. [11], p. 262 for a discussion of the balance equation for $\overline{c^2}$). Consequently, $\overline{c^2}/\varepsilon_c$ decreases downstream of the patch because ε_c, the dissipation of $\overline{c^2}$ by molecular action, occurs in the fine scale motions which respond only slowly to changes in the mean field. In the present scheme $\overline{c^2}/\varepsilon_c$ is assumed proportional to k/ε which is entirely *unaffected* by the scalar field, and as a result the use of equation (8) will produce values for $\phi_{ic.1}$ which are smaller than if $\overline{c^2}/\varepsilon_c$ had been available for use as a time scale. Now, $\phi_{ic.1}$ is effectively the sink term in the $\overline{u_i c}$ equation: it is thus the process which prevents the scalar flux correlation from growing indefinitely. So if the sink term is too small, the scalar fluxes will be too large, leading in turn to the observed too rapid rate of spread. When we began the present study the uncertainties and obstacles in formulating a diagnostic transport equation for ε_c seemed sufficiently formidable to make us explore first how far one could get without it. Its development, however, now seems appropriate.

Improvements in the modelling of the other pressure-interaction and diffusion processes in equation (6) can doubtless be devised in the next few years. At present, however, defects in predicting the scalar field often spring principally from shortcomings in the *hydrodynamic* model. This is certainly the case for the plane wake and is at least partly so for the mixing layer with a stagnant stream. An inference is that even those ultimately interested only in the scalar field may need to focus on improving the Reynolds stress and dissipation equations to obtain a sufficiently reliable scalar-flux predictor.

Finally, the large and initially surprising error in the log-law thermal boundary condition that is evident in Fig. 17 helps to emphasize that practically nothing is yet known about the scalar transport mechanisms in the immediate near-wall region. This is an area where sustained research over a number of years will be needed to achieve a satisfactory level of comprehension.

Acknowledgements—The work has been supported by the U.K. Science Research Council through grant B/RG/78011 and by the U.S. Department of Energy (Division of Basic Energy Sciences) under contract W-77405-ENG-48. The help of Ms. L. S. Majesky in preparing the manuscript for publication is gratefully acknowledged.

Authors' names appear alphabetically.

REFERENCES

1. B. E. Launder and D. B. Spalding, *Mathematical Models of Turbulence*. Academic Press, London (1972).
2. B. J. Daly and F. H. Harlow, Transport equations in turbulence, *Physics Fluids* **13**, 2634 (1970).
3. C. du P. Donaldson, A progress report on an attempt to construct an invariant model of turbulent shear flows, *Proc. AGARD Conf. on Turbulent Shear Flows*, London, Paper B-1, AGARD CP-93 (1972).
4. B. E. Launder, G. J. Reece and W. Rodi, Progress in the development of a Reynolds-stress turbulence closure, *J. Fluid Mech.* **68**, 537 (1975).
5. J. C. Wyngaard and O. R. Cote, The evolution of a convective planetary boundary layer—A higher order closure model study, *Bound-Layer Meteorol.* **7**, 289 (1974).
6. J. L. Lumley and O. Zeman, Buoyancy effects in entraining turbulent boundary layers: A second order closure study, in *Turbulent Shear Flows—I*, p. 295. Springer, Berlin (1979).
7. C. du P. Donaldson, R. D. Sullivan and H. Rosenbaum, A theoretical study of the generation of atmospheric-clear air turbulence, *AIAA J.* **10**, 162 (1972).
8. M. M. Gibson and B. E. Launder, Ground effects on pressure fluctuations in the atmospheric boundary layer, *J. Fluid Mech.* **86**, 491 (1978).
9. R. G. Owen, An analytical turbulent transport model applied to non-isothermal fully-developed duct flows, Ph.D. Thesis, The Pennsylvania State University (1973).
10. B. E. Launder and D. S. A. Samaraweera, Application of a second-moment turbulence closure to heat and mass transport in thin shear flows—II. Three-dimensional convection (In press).
11. B. E. Launder, Heat and mass transport, in *Turbulence—Topics in Applied Physics*, Vol. 12, edited by P. Bradshaw, Springer, Berlin (1976).
12. A. S. Monin, On the symmetry properties of turbulence in the surface layer of air, *Izv. Atmos. Oceanic Phys.* **1**, 45 (1965).
13. B. E. Launder, Scalar property transport by turbulence, Rep. No. HTS/73/26 Dept. Mech. Engr., Imperial College, London (1973).
14. B. E. Launder, On the effects of a gravitational field on the turbulent transport on heat and momentum, *J. Fluid Mech.* **67** (3), 569 (1975).
15. S. V. Patankar and D. B. Spalding, Heat and mass transfer laws for fully turbulent wall flows, *Int. J. Heat Mass Transfer* **15**, 2329 (1972).
16. B. E. Launder and A. Morse, A numerical prediction of axisymmetric free shear flows with a second-order Reynolds stress closure, *Proc. First Turbulent Shear Flow Symposium*, The Pennsylvania State University (1977).
17. C. L. V. Jayatilleke, The influence of Prandtl number and surface roughness on the resistance of the laminar sublayer to momentum and heat transfer, *Prog. Heat Mass Transfer* **1**, 193 (1959).
18. B. G. Van Der Hegge Zijnen, Measurements of turbulence in a plane jet of air by the diffusion method and by the hot-wire method, *Appl. Sci. Res.* **7A**, 293 (1958).
19. P. E. Jenkins and V. W. Goldschmidt, Mean temperature and velocity in a plane turbulent jet, *J. Fluids Eng., Trans. ASME* **95**, 581 (1973).
20. A. A. Townsend, The fully developed turbulent wake of a circular cylinder, *Aust. J. Scient. Res.* **2A**, 451 (1949).
21. G. Fabris, Turbulent temperature and thermal flux characteristics in the wake of a cylinder, *Proc. First Turbulent Shear Flow Symposium*, The Pennsylvania State University (1977).
22. W. E. Watt, The velocity–temperature mixing layer, Rep. No. TP 6705, Dept. Mech. Engr., University of Toronto (1967).
23. W. Rodi, A review of experimental data of uniform density free turbulent boundary layers, in *Studies in Convection—Theory, Measurements and Applications*, Vol. 1, edited by B. E. Launder. Academic Press, London (1975).
24. M. Sunyach and J. Mathieu, Zone de mélange d'un jet

intermittence, *Int. J. Heat Mass Transfer* **12**, 1679 (1969).
plan fluctuations induites dans le cone à potential-
25. D. S. A. Samaraweera, Turbulent heat transport in two- and three-dimensional temperature fields, Ph.D. Thesis, University of London (1978).
26. J. Laufer, The structure of turbulence in fully-developed pipe flow, NACA Rep. 1174 (1954).
27. C. J. Lawn, The determination of the rate of dissipation in turbulent pipe flow, *J. Fluid Mech.* **48**, 477 (1971).
28. K. Bremhorst, and K. J. Bullock, Spectral measurements of temperature and longitudinal velocity fluctuations in fully developed pipe flow, *Int. J. Heat Mass Transfer* **13**, 1313 (1970).
29. K. Bremhorst and K. J. Bullock, Spectral measurements of turbulent heat transfer in fully-developed pipe flow, *Int. J. Heat and Mass Transfer* **16**, 2141 (1973).
30. J. Rotta, Turbulent boundary layers in incompressible flow, in *Progress in Aeronautical Science*, Vol. 2. Pergamon, Oxford (1962).
31. A. Quarmby and R. K. Anand, Axisymmetric turbulent mass transfer in a circular tube, *J. Fluid Mech.* **38**, 433 (1969).
32. R. A., Antonia, H. Q. Danh and A. Prabhu, Response of a turbulent boundary layer to a step change in surface heat flux, *J. Fluid Mech.* **80**, 153 (1977).
33. A. K. Kudva and A. Sesonske, Structure of turbulent velocity and temperature fields in ethylene glycol pipe flow at low Reynolds number, *Int. J. Heat and Mass Transfer* **15**, 127 (1972).
34. W. P. Jones and B. E. Launder, Some properties of sink-flow turbulent boundary layers, *J. Fluid Mech.* **56**, 357 (1972).
35. L. Fulachier, Contribution a l'étude des analogies des champs dynamique et thermique dans une couche limite turbulente, Effect de l'aspiration, thèse Docteur es Sciences, Université de Provence (1972).
36. J. Blom, An experimental determination of the turbulent Prandtl number in a developing temperature boundary layer, Ph.D. Thesis, The Technological University, Eindhoven (1970).
37. J. L. Lumley, Computational modeling of turbulent flows, *Advances in Applied Mechanics*, Vol. 18, pp.123–126. Academic Press, New York (1978).

APPLICATION D'UNE FERMETURE DE SECOND MOMENT AU TRANSPORT TURBULENT DE CHALEUR ET DE MASSE DANS DES ECOULEMENTS A CISAILLEMENT MINCE I—TRANSPORT BIDIMENSIONNEL

Résumé—On développe une approximation de second moment pour la convection turbulente dans laquelle les flux thermiques turbulents forment eux-même la base d'un système d'équations de transport. A ce niveau, la fermeture nécessite la formulation du nombre de Prandtl turbulent qui est l'incertitude empirique principale. On donne des applications à une variété d'écoulements à cisaillement et à couche limite. Tandis qu'on obtient un bon accord, le modèle ne peut rendre compte complètement des variations observées du nombre de Prandtl turbulent d'un écoulement à l'autre et aussi il donne des résultats plutôt imprécis en aval d'une courte tache chaude sur une paroi.

ANWENDUNG EINES DREHIMPULS-TURBULENZ-MODELLS AUF WÄRME- UND STOFFTRANSPORT IN DÜNNEN SCHERSTRÖMUNGEN

Zusammenfassung—Dieser Beitrag beschreibt die Entwicklung einer Drehimpuls-Näherung für turbulente Konvektion, wobei die turbulenten Wärmeströme selbst Gegenstand der Behandlung in einem Satz von Transportgleichungen sind. Ein Abschluß auf dieser Ebene vermeidet die Notwendigkeit, die turbulente Prandtl-Zahl vorschreiben zu müssen, die bei einfacheren Behandlungen die größte empirische Unsicherheit darstellt. Über die Anwendungen auf den Wärmetransport in einer Vielzahl von freien Scherströmungen und Grenzschichten wird berichtet.

ПРИМЕНЕНИЕ МОМЕНТНОЙ МОДЕЛИ ВТОРОГО ПОРЯДКА К ИССЛЕДОВАНИЮ ТУРБУЛЕНТНОГО ТЕПЛО- И МАССОПЕРЕНОСА В ТОНКИХ СДВИГОВЫХ ПОТОКАХ: ДВУХМЕРНЫЙ СЛУЧАЙ

Аннотация — В работе представлено приложение модели второго порядка к рассмотрению процессов турбулентного переноса. В этом случае турбулентные потоки тепла определяют форму уравнений для моментов. Замыкание уравнений на уровне модели второго порядка позволяет не прибегать к заданию турбулентного числа Прандтля, что принципиально вносит эмпирическую неопределенность на более низком уровне моделирования турбулентного переноса. Рассмотрен ряд задач турбулентного переноса в свободных и пристенных течениях. Хотя результаты расчета находятся в достаточно хорошем согласии с опытом, однако предложенная модель недостаточно удовлетворительно описывает турбулентное число Прандтля для различных течений и дает неверные результаты для течения за коротким нагретым участком.